Influence of multiple detection events on compositional accuracy of TiN coatings in atom probe tomography

Surface & Coatings Technology 477 (2024) 130318

Contents lists available at ScienceDirect

Surface & Coatings Technology

journal homepage: www.elsevier.com/locate/surfcoat

Full length article

Influence of multiple detection events on compositional accuracy of TiN coatings in atom probe tomography

Maximilian Schiester [a,*], Helene Waldl [a], Marcus Hans [b], Mattias Thuvander [c], Daniel Primetzhofer [d], Nina Schalk [a], Michael Tkadletz [e]

[a] Christian Doppler Laboratory for Advanced Coated Cutting Tools at the Department of Materials Science, Montanuniversität Leoben, Franz-Josef-Straße 18, 8700 Leoben, Austria
[b] Materials Chemistry, RWTH Aachen University, Kopernikusstraße 10, 52074 Aachen, Germany
[c] Department of Physics, Chalmers University of Technology, 41296 Göteborg, Sweden
[d] Department of Physics and Astronomy, Uppsala University, Lägerhyddsvägen 1, 75120 Uppsala, Sweden
[e] Department of Materials Science, Montanuniversität Leoben, Franz-Josef-Straße 18, 8700 Leoben, Austria

ARTICLE INFO

Keywords:
Atom probe tomography
TiN
Compositional accuracy
Multiple detection events
Electric field strength

ABSTRACT

The accuracy of composition measurements by atom probe tomography is often dependent on the selected operation mode as well as the applied measurement parameters. The detected hit characteristics, distinguishing between single and multiple events, along with the electric field, are also affected by parameter selection. In this study, atom probe tomography experiments were performed on a stoichiometric TiN coating in voltage as well as in laser-assisted mode with systematically varied laser pulse energies. The observed elemental compositions were compared with complementary ion beam analysis measurements. The influence of multiple detection events was investigated by two approaches: I) A modified local electrode served as a hardware filter, reducing multiple detection events from 78.8 % to 41.9 % and from 40.9 % to 5.6 % using voltage mode and laser-assisted APT (0.6 nJ), respectively, and II) unfiltered datasets were analyzed by data post processing. The latter allowed the study of ion species, particularly of emerging complex molecular ions associated with dissociation processes. Additionally, average electric fields were estimated and spatial considerations were made to investigate the evolution of charge state ratios and hit characteristics during the measurement. Filtering the measurements significantly improved the elemental accuracy. In voltage mode, hardware and software filtering reduced the discrepancy between reference and observed composition from 3.8 at.% to 2.1 at.% and 0.1 at.% within uncertainty limits. In laser-assisted mode, higher laser pulse energy increased the difference between unfiltered data and the reference composition, from 1.4 at.% (0.1 nJ) to 8.1 at.% (2.0 nJ). Ion species analysis of the datasets shows an increasing presence of complex ions (Ti_2N) with raising laser pulse energy. Electric field studies reveal a decline from 40 V/nm in voltage mode to 36 V/nm applying a high laser pulse energy of 2.0 nJ, indicating insufficient field strength for neutral nitrogen re-ionization.

1. Introduction

Atom probe tomography (APT) is a unique characterization technique, which allows to detect and visualize the three-dimensional distribution of elements with almost atomic resolution. The fundamental principle is based on the work of Müller [1] from 1956, the metrology was introduced a few years later [2]. APT opens up a variety of new possibilities to investigate e.g. nanoscale materials, functional thin films or wear-resistant coatings [3]. The introduction of laser-assisted APT made it possible to study materials with low electric conductivity and even insulators [4]. However, quite often the obtained accuracy in composition is highly dependent on the used measurement parameters [5–14] In particular, for binary nitrides, such as TiN, GaN, AlN or CrN, a pronounced effect of the applied laser pulse energy (LPE) and thus, also of the local electric field on the obtained elemental composition was repeatedly reported [15–20]. For GaN, a wide range of results was observed when applying different LPEs, ranging from an overestimation [21] to an underestimation of the N content of up to 30 at.% [22]. If two or more ions are evaporated during the same pulse and reach the detector, they will be recorded as a multiple detection event. It is well

* Corresponding author.
E-mail address: maximilian.schiester@unileoben.ac.at (M. Schiester).

https://doi.org/10.1016/j.surfcoat.2023.130318
Received 14 September 2023; Received in revised form 14 December 2023; Accepted 15 December 2023
Available online 17 December 2023

known that nitrides tend to exhibit a significant fraction of multiple detection events for which associated effects such as the ion pile-up phenomenon, a detector limitation, can severely affect the accuracy of the elemental composition [20,23–25]. Hence, the grid LE was intentionally employed to minimize ion pile-up phenomena. Extensive studies on GaN [16,21,22], TiAlN [5,6] and CrN [15] revealed a strong N-deficiency utilizing insufficient electric fields, i.e. high LPEs, which was related to undetectable neutrals upon dissociation processes of molecular ions [26].

In the present work, the accuracy of the evaluated elemental composition of APT measurements of a stoichiometric sputter-deposited TiN coating was systematically investigated. For this purpose, voltage and laser-assisted measurements, applying different field evaporation conditions, were performed. The influence of multiple detection events on the elemental composition was investigated with two different approaches of filtering different detection events. I) An adapted hardware filtering set-up i.e. a local electrode (LE) with a grid (grid LE) placed in the flightpath between specimen and detector, which consequently stops a part of neighboring ions, thus, effectively reducing multiple detection events [20,27,28]. II) Ex-situ software filtering was used to completely remove the multiple detection events from datasets acquired with a standard local electrode (standard LE) in a data post processing step. In addition, the influence of the LPE and the associated change in the electric field strength on the detection events was also studied in order to obtain a thorough understanding of the predominant physical phenomena during field evaporation of TiN.

2. Experimental methods

The TiN coating investigated in this work was synthesized by reactive, unbalanced magnetron sputtering using a CemeCon CC800/9MLT industrial-scale sputter deposition system. Single crystalline Si strips with (100) orientation, manufactured by CrysTec, were used as substrate. Prior to deposition, the Si substrates were cleaned with acetone and ethanol in an ultrasonic bath. After mounting in the deposition chamber and evacuation, the strips were exposed to an Ar^+ plasma etching step. At 550 °C, deposition of the TiN coating with a thickness of about 5 μm was carried out in Ar/N_2 atmosphere, further details on the synthesis can be found in Ref. [29]. The TiN coating has a face centered cubic crystal structure (NaCl-type, space group 225).

As basis for the comparison of the influence of APT measurement parameters on the compositional accuracy, the elemental composition of the TiN coating was determined by two complementary ion beam based analysis techniques at the 5 MV NEC Pelletron tandem accelerator at the Tandem Laboratory at Uppsala University, Sweden [30]. Time-of-flight elastic recoil detection analysis (ToF-ERDA) using 36 MeV I^{8+} primary ions and Rutherford backscattering spectrometry (RBS) using 2 MeV He^+ primary ions, were employed to quantify the reference composition of the TiN coating. The ToF-ERDA/RBS measurements yielded an elemental composition of 49.6 ± 1.5 at.% Ti and 50.4 ± 1.5 at.% N. Details on the experiment as well as the underlying uncertainties in the combined approach are discussed extensively in Moro et al. [31]. On average 0.1 at.% O content was measured, this was neglected and solely the Ti and N contents were considered. Within the limits of uncertainty, a stoichiometric composition could be concluded from those results, further details on the measurements as well as the measurement data can be found in Ref. [32].

Needle-shaped atom probe specimens were prepared by focused ion beam (FIB) milling using Ga^+ ions in a FEI Versa 3D DualBeam SEM/FIB workstation. A standard lift-out [33] was performed to extract a rectangular-shaped lamella from the sample and pieces of the lamella were attached to prefabricated posts on a microtip coupon. Subsequently, the specimens were prepared via annular milling, following the procedure according to [34]. The final shaped specimens exhibited a tip radius below 50 nm.

All APT measurements shown within the present work were carried out with a CAMECA LEAP 3000X HR atom probe, equipped with a 532 nm (green) – 10 ps pulsed laser. The base temperature was kept constant at 60 K for all measurements. The measurement in voltage mode utilizing the standard LE was performed with 200 kHz pulse rate, 20 % pulse fraction and 1 % detection rate. For the measurements using the hardware filter similar parameters were applied, only the detection rate was reduced to 0.15 % to comply with the lower detection efficiency caused by the grid LE. As a result of the considerably reduced open area of the grid LE, the detection efficiency of a LEAP 3000X HR drops from 37 % using the standard LE to 5 %, which corresponds to a factor of 7.4, when the hardware filter is used [27]. For the measurements with the grid LE, the DR was accordingly adjusted to maintain a roughly comparable evaporation rate. This not only prevents a possible loss of data quality, but above all protects the specimen from excessive stress. For the laser-assisted APT measurements, the pulse rate was kept constant at 250 kHz. Similar to the voltage mode measurements, a detection rate of 1 % and 0.15 % were used with the standard LE and hardware filter, respectively. For the parameter variation, the LPE was increased from 0.1 to 0.5, 1.0, 1.5 and 2.0 nJ. For filtering multiple detection events, two different laser pulse energies were used to analyze and compare the effectiveness of the two filtering methods, a moderate LPE of 0.6 nJ and a high LPE of 1.5 nJ.

The reconstruction of the herein acquired data was performed using the "Integrated Visualization and Analysis Software" IVAS 3.6.14 from CAMECA. In order to minimize the influence of thermal tails with increasing laser pulse energy, considerable emphasis was laid on selecting peak ranges symmetrically around the peak maximum, starting with the first noticeable deviation from the background level, when ranging the mass spectra [5]. In addition to the main elements Ti and N, the elements Al, Ar, C, Ga, O as well as molecular ions such as TiON were also found, but their contribution to the overall elemental composition was below 1 at.% in all measurements. All mass spectra (Fig. S1-S14) as well as an overview of the assigned ion species (Table S1) can be found in the supplementary material.

For ex-situ software filtering, the .epos files (i.e. extended.pos files) of the measurements using a standard LE were utilized. Among others, the number of ions per pulse and thus, the information whether a hit is a single or multiple detection event, is saved. Based on the.epos files, a module was programmed with Python (3.9.5), which reads in the dataset, extracts the multiple detection events, i.e. filtering, and then exports it as a.pos file. The data are stored as 4-byte float and unsigned integer in big-endian byte order, which makes a byte swap necessary on most operating systems. In addition to the single detection events, the previously removed multiple detection events were also exported as part of the analysis. Using the Python module, all measurements were filtered and then re-analyzed using the range file of the original measurement. In the process of filtering, it was possible to determine the exact number of all detection events and thus, the proportion of multiple detection events. For the filtered measurements, an apparent detection efficiency was calculated, which is the product of the detection efficiency of the standard LE (i.e. 37 %) and the percentage of the remaining single detection events.

3. Results and discussion

3.1. Influence of filtering multiple detection events in voltage-assisted APT

The evolution of the standing voltage and the background during the voltage mode measurements using the standard LE and the hardware filter, are presented in Fig. 1a. It is noticeable that the background during the measurement applying the hardware filter was considerably higher (avg. 60 ppm/ns) than with the standard LE (avg. 14 ppm/ns), while the standing voltages showed a very similar evolution. These two observations can be made in all measurements shown within this work. In Fig. 1b-c, the results of the compositional analysis and corresponding share of multiple detection events of the performed filtering approaches

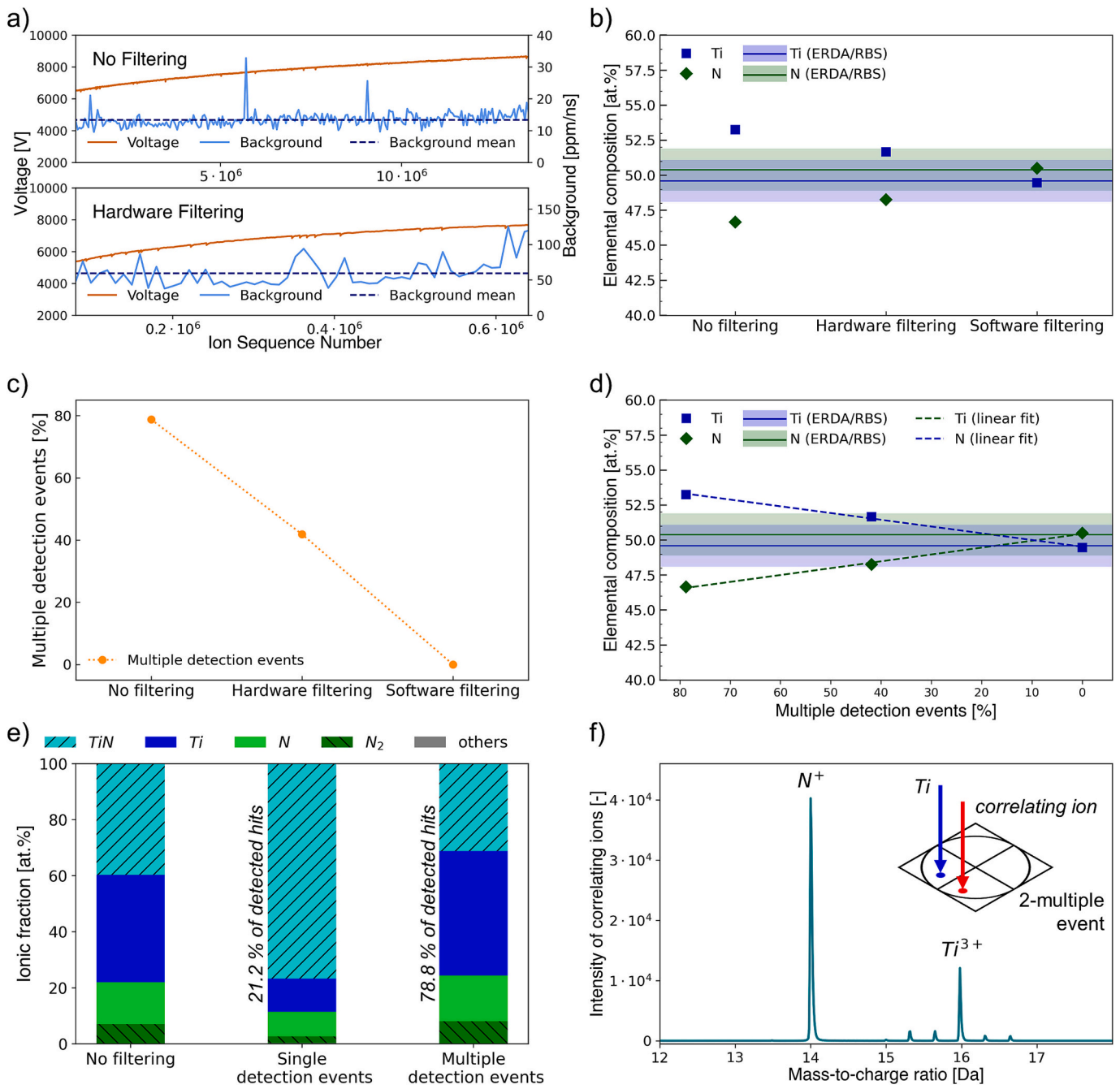

Fig. 1. (a) Voltage and background evolution as a function of the ion sequence applying no filtering and hardware filtering. (b) Results of the elemental composition of filtering multiple detection events in voltage mode APT and (c) corresponding share of multiple detection events. (d) The linear relationship between elemental composition and the share of multiple detection events. (e) Corresponding analysis of detector events with respect to the ion species. (f) Ion correlation spectrum representing the ions forming a 2-multiple event, i.e. a multiple detection event consisting of two hits, together with a Ti (3+, 2+ or +) ion. No additional peaks exist outside the range shown.

can be seen. The evaluation of the measurement using the standard LE, in which the majority of the hits (78.8 %) were detected as multiple detection events, resulted in a relatively high deviation from the reference elemental composition and the N content is underestimated by 3.8 at.%. When using the hardware filter, the proportion of multiple detection events was roughly halved from 78.8 to 41.9 % and the accuracy of elemental composition was significantly improved, the deviation of the N content was reduced to 2.1 at.%. Probably due to hydrophilic properties of the adhesive used in the grid LE to fix the grid, pronounced peaks at 8 (O^{2+}) and 18 Da (H_2O^+) were detected, which can be attributed to contamination of the grid LE with water. This contribution could not be completely removed despite treatment with a plasma cleaner, as suggested by Larson et al. [35]. This circumstance may also explain the increased background level during the measurement. However, these impurities were neglected for analysis of the elemental composition since ToF-ERDA/RBS data did not show significant amounts of H and O present in the TiN coating. Hence, the Ti/N ratio was used as a basis for the elemental composition obtained by the hardware filter measurement. In the reconstruction of the software filtered measurement using the standard LE, within the limits of uncertainty due to counting statistics [5], a similar composition as observed via ToF-ERDA/RBS was obtained. Table 1 gives an overview

Table 1
Results of filtering multiple detection events of voltage mode measurements.

	No filtering	Hardware filtering	Software filtering
N [at.%]	46.7	48.3	50.5
Ti [at.%]	53.3	51.7	49.5
Total evaluated hits	4.4×10^6	0.6×10^6	0.9×10^6
Detection efficiency [%]	37	5	7.9[a]
Overall evaporated ions[b]	11.9×10^6	12.0×10^6	11.9×10^6
Multiple detection events [%]	78.8	41.9	0

[a] Apparent detection efficiency.
[b] Estimated number of evaporated ions based on detection efficiency.

about the contents of Ti and N, the number of evaluated hits as well as the share of multiple detection events of the different filtering approaches. Based on the different detection efficiencies, care was taken to evaluate the same number of overall evaporated ions, i.e. the identical volume, of approximately 12 million ions. Apparently, for voltage mode measurements, the compositional accuracy increases steadily with decreasing number of multiple detection events. This observation has already been described by Thuvander et al. [27] for carbides in steels. In Fig. 1d, the elemental composition is shown as a function of the share of multiple detection events, revealing a linear relationship. Although, the software filtering leads to a poor apparent detection efficiency of ~8 %, a recently published study has shown that the influence of this relatively low apparent detection efficiency on the investigation of small particles or solute clusters is marginal in comparison to other limiting factors, such as effective spatial resolution [36]. Thus, in terms of elemental composition, software filtering as well as hardware filtering appear to be useful tools to obtain accurate composition data. Nevertheless, it should be mentioned that the low detection rate of 8 % in case of hardware filtering provides much less data, resulting in a significant loss of information. Although the detector in the LEAP 3000X HR used here is already equipped with a third delay line, resulting in improved multihit resolution, newer instruments may provide even better results [11]. The major advantage of software-based filtering is the applicability to any measurement, while still the full amount of achievable data given by the actual detection efficiency of the used instrument is available. It should be noted that the findings for nitrides are not necessarily transferable to other compounds, such as carbides, oxides or borides [18,28].

In order to investigate the reason why software filtering of the measurements leads to such a significant improvement in compositional accuracy, the filtered fraction of detected ions (i.e. multiple detection events) was also analyzed. The original measurement containing all detector events was compared with the single detection events and the previously filtered multiple detection events, the results can be seen in the bar chart in Fig. 1e. A closer analysis of the multiple detection events reveals a significantly higher proportion of Ti, a corresponding loss of N and a lower proportion of TiN, compared to the single detection events. This difference is probably due to dissociation processes during field evaporation, which will be discussed below. From the bar chart, the influence of the different detection events on the elemental composition can be directly deduced. For this purpose, the atom number ratio $(n_N + 2n_{N_2})/n_{Ti}$ was considered, where value 1 would mean stoichiometric TiN. Large amounts of molecular TiN shift the elemental composition further in the direction of stoichiometry, they do not contribute to the deviation and were therefore neglected in the atom number ratios. For the single detection events, this ratio is 1.12, whereas it is 0.72 for the multiple detection events. The relatively high proportion of multiple detection events and the small ratio lead to a significant underestimation of the N content in the unfiltered measurement.

The nature of dissociation processes of molecular ions can be visualized using ion correlation histograms [37]. It is usually assumed that in datasets acquired with reflectron-based instruments, such as the here employed LEAP 3000X HR, dissociation processes cannot be visualized as dissociation tracks in the histogram due to the energy compensation by the reflectron [37,38]. An ion correlation histogram evaluation of the voltage mode measurement also showed no evidence of dissociation tracks. Nevertheless, an attempt to analyze the dissociation $TiN \rightarrow Ti + N$ is shown in Fig. 1f. For this purpose, all multiple detection events with two ions, often referred to as 2-multiple events, in which one of the ions is Ti (1+,2+,3+), were investigated. The corresponding ions of the detected pairs form a mass spectrum, hereafter referred to as ion correlation spectrum. It shows a maximum at 14 Da and marks the N^+ peak, suggesting the occurrence of two different effects: One being co-evaporation, where the evaporation of an ion triggers that of another, and secondly that a fraction of the multiple detection events is a result of dissociation processes, in which some N may be lost in the form of undetectable neutrals, due to N—N recombination. Furthermore, the five distinctive peaks of Ti^{3+} are recognizable, equivalent to Ti—Ti multiple detection events, which may be due to pile-up phenomena, hardware limitations by the detector, and caused by co-evaporation [20,39]. The spectrum shows no further peaks above 20 Da. Thus, a low fraction of multiple detection events is preferable to achieve accurate results, which can be obtained either by careful parameter selection or by filtering.

3.2. Laser pulse energy variation

While the data from the LPE variation have been partially already reported in a recent publication [32], the present work is focused on the different hit characteristics, i.e. single and multiple detection events. Fig. 2a shows the standing voltage and the background during the LPE variation measurement, where it can be seen that with increasing LPE, less voltage is required to maintain a constant detection rate and also the

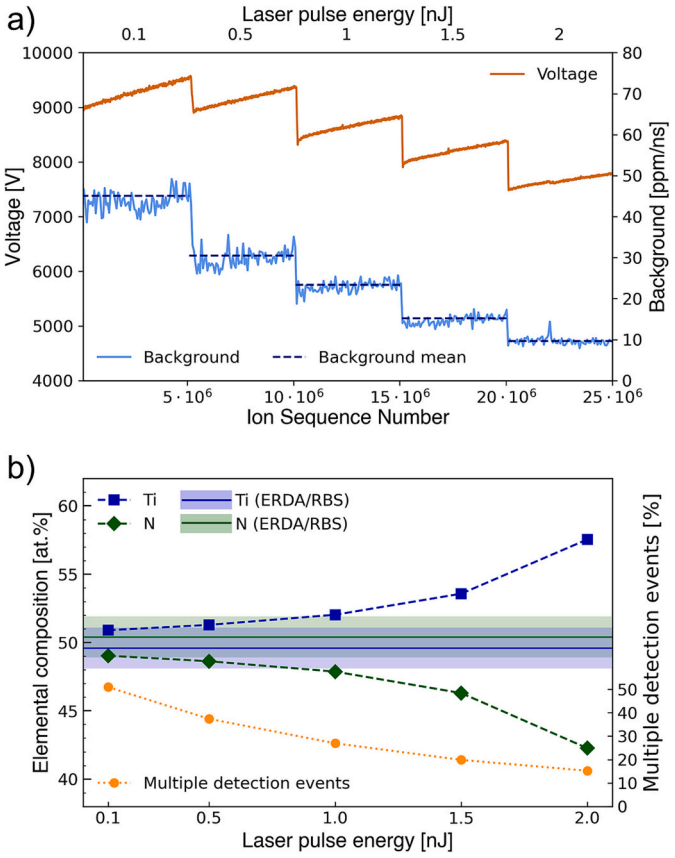

Fig. 2. (a) Standing voltage and background history with respect to the laser pulse energy and (b) results of elemental composition and share of multiple detection events.

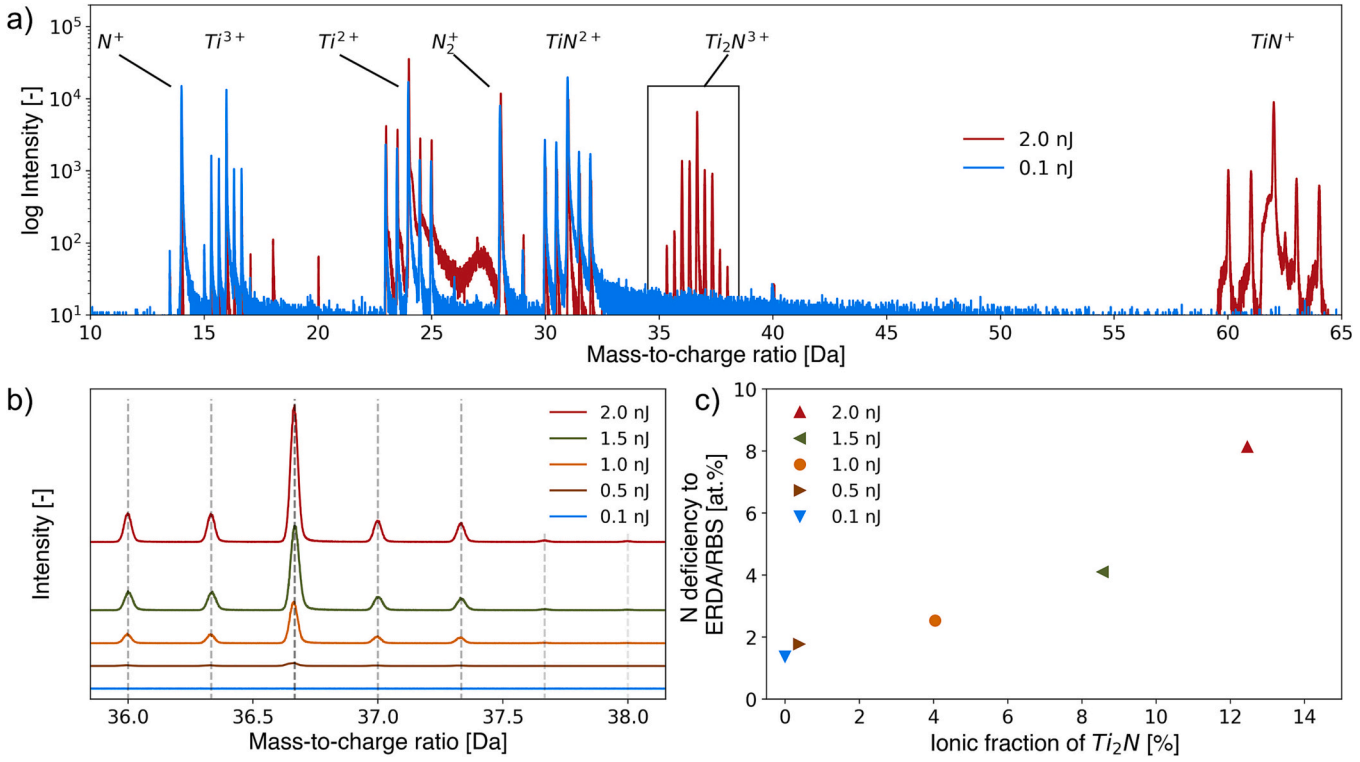

Fig. 3. (a) Mass spectra for laser pulse energies of 0.1 (blue line) and 2.0 nJ (red line). (b) Detail of the evolution of the Ti_2N^{3+} peaks with increasing laser pulse energy during the variation and (c) the growing N deficiency as a function of the increasing Ti_2N fraction. (For interpretation of the references to color in this figure legend, the reader is referred to the web version of this article.)

background decreases significantly. To ensure comparability, for each LPE about 5 million ions were acquired. The results of elemental composition, as well as the fraction of multiple detection events, are presented in Fig. 2b. The lowest LPE, 0.1 nJ, yielded an N concentration of 49.0 at.%, while at the highest LPE of 2.0 nJ only 42.3 at.% N were detected. Comparison with ToF-ERDA/RBS results shows an increasing N underestimation from 1.4 at.% (0.1 nJ) up to 8.1 (2.0 nJ) at.% with increasing LPE. In the above studied voltage mode measurements, the increasing discrepancy was coinciding with a higher proportion of multiple detection events. However, for the laser pulse energy variation studied here, the fraction of multiple detection events decreased with increasing LPE, while the underestimation of the N content increased with increasing LPE. Thus, as reported for (Ti,Al)N films [5], it is unlikely that the significant underestimation with increasing LPE is solely related to multiple detection events. Consequently, other physical phenomena are assumed to be present, which will be discussed in the following.

In Fig. 3a the two mass spectra of the measurements with LPEs of 0.1 as well as 2.0 nJ are compared. In addition, a detailed view of the evolution of the Ti_2N^{3+} peaks with increasing LPE can be seen in Fig. 3b. Ti_2N is a complex molecular ion and the fraction increases from 0 % (0.1 nJ) to 12.5 % (2.0 nJ), suggesting that the increased laser energy promotes dissociation processes associated with a reduced electric field [26]. This effect of thermal pulsing is emphasized by the strong correlation of N underestimation with the Ti_2N fraction in Fig. 3c. The spectrum of the measurement with 2.0 nJ LPE further reveals TiN^+ peaks at 60–64 Da, while a decrease of the Ti^{2+} peaks can be observed. The observation of ions with low charge states can be attributed to lower electric field strengths.

3.3. *Influence of filtering multiple detection events in laser-assisted APT*

For the study of multiple detection events in laser-assisted APT, the filtering approaches were applied using two different LPEs. Figs. 4a-d show the standing voltage evolution and background curves for the standard LE and hardware filtering measurements, respectively, as well as the results of the elemental compositions of the reconstructions and the fraction of multiple detection events, at moderate 0.6 nJ and high 1.5 nJ LPE. By applying a moderate LPE, as is evident from the results presented in Fig. 4c, a high compositional accuracy and a relatively low background could be obtained and therefore filtering exhibited no effect within the limits of accuracy. Nevertheless, the data obtained by software filtering provide a solid basis for analyzing changes in the composition of single and multiple detection events associated with the change in laser pulse energy. In Tables 2 and 3, in addition to the elemental compositions, statistics of the reconstructions are also given. At 1.5 nJ LPE, it is known from the data presented in Section 3.2 that there is an underestimation of the N content of 4.1 at.%, which could be reduced to 3.4 at.% using the hardware filter and 2.6 at.% with software filtering, respectively. A significant reduction, but not sufficient to yield proper results. Hence, the assumption made in the previous section, that the influence of multiple detection events in laser-assisted APT is minor, is confirmed and suggests additional other physical phenomena to be present. The study by Santhanagopalan et al. [13] demonstrates that when operating in laser-assisted mode, differences in chemical composition and selective element loss occur in relation to laser energy and wavelength.

In Fig. 5a and b the bar graphs show fractions of the encountered ion species, separated according to the type of detection event for the moderate and high laser pulse energy measurements using a standard LE. When using a moderate LPE, it can be observed that the proportion of Ti ions is about twice as large as that of the molecular N_2 ions. Together with the low occurrence of complex molecular ions, this is responsible for the high accuracy of the elemental composition. Due to the high LPE, more complex Ti-rich ions were observed (i.e. Ti_2N), which were preferentially detected as single detection events. Similar to the comparison of the filter approaches in voltage mode, an atom number ratio $(n_N + 2n_{N_2} + n_{Ti_2N})/(n_{Ti} + 2n_{Ti_2N})$ was calculated for the

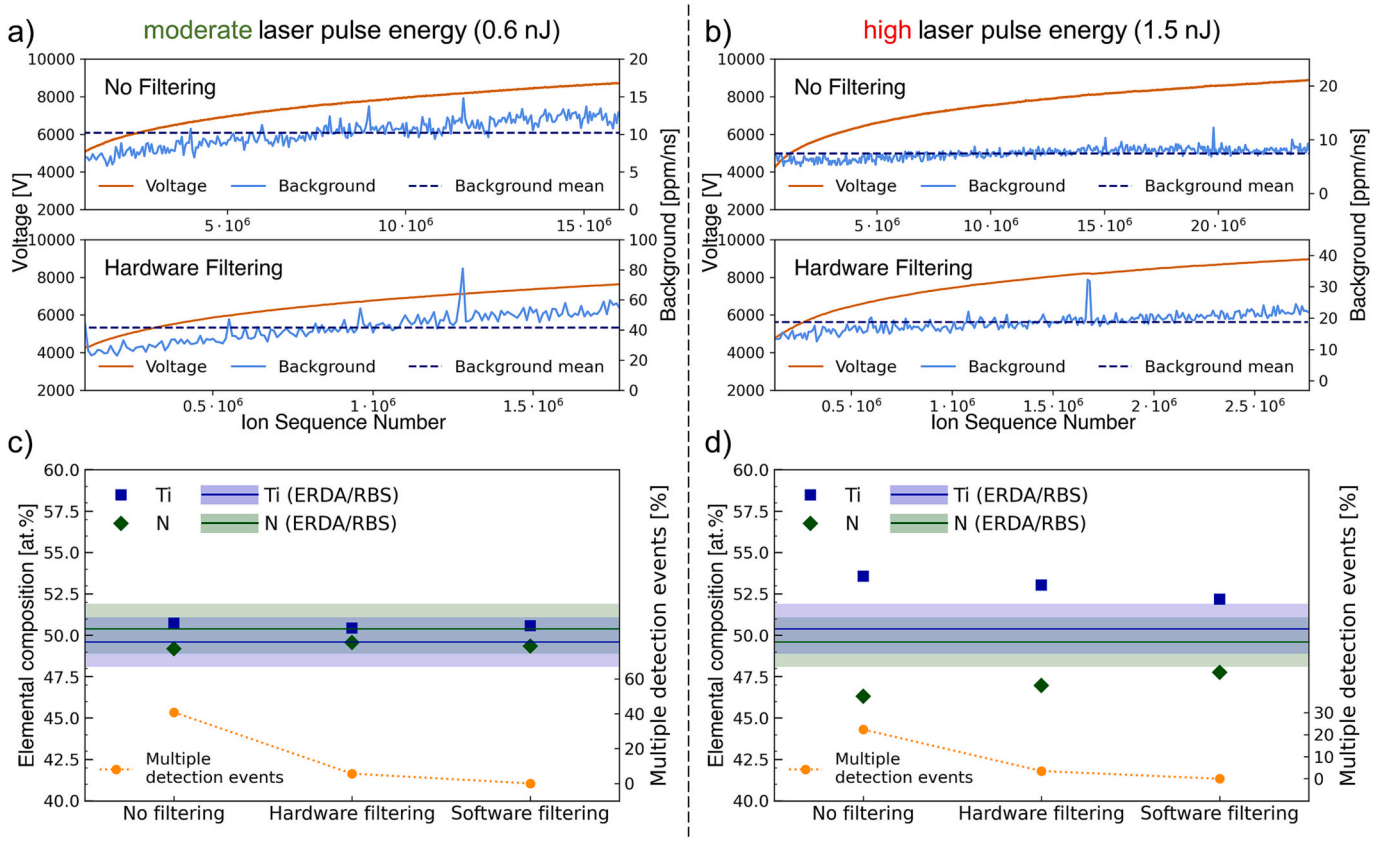

Fig. 4. Voltage and background history of measurements using (a) low and (b) high laser pulse energy, and (c-d) the associated results of filtering multiple detection events.

Table 2
Results of filtering multiple detection events of laser-assisted measurements maintaining a moderate LPE of 0.6 nJ.

	No filtering	Hardware filtering	Software filtering
N [at.%]	49.2	49.6	49.4
Ti [at.%]	50.8	50.4	50.6
Total evaluated hits	14.5×10^6	1.8×10^6	8.6×10^6
Detection efficiency [%]	37	5	21.9[a]
Overall evaporated ions[b]	39.2×10^6	36.0×10^6	39.3×10^6
Multiple detection events [%]	40.9	5.6	0

[a] Apparent detection efficiency.
[b] Estimated number of evaporated ions based on detection efficiency.

Table 3
Results of filtering multiple detection events of laser-assisted measurements maintaining a high LPE of 1.5 nJ.

	No filtering	Hardware filtering	Software filtering
N [at.%]	46.3	47.0	47.8
Ti [at.%]	53.7	53.0	52.2
Total evaluated hits	23.6×10^6	2.7×10^6	18.3×10^6
Detection efficiency [%]	37	5	28.7[a]
Overall evaporated ions[b]	63.8×10^6	54.0×10^6	63.8×10^6
Multiple detection events [%]	22.3	3.5	0

[a] Apparent detection efficiency.
[b] Estimated number of evaporated ions based on detection efficiency.

high laser pulse energy (1.5 nJ), which provides information on how the two different types of detector events affect the stoichiometry. Similar to the evaluation of the voltage mode measurements, the TiN counts were also neglected here, as they do not contribute to the deviation from the stoichiometric composition. For the single detection events this ratio is 0.81, and a ratio of 0.44 is obtained for the multiple detection events, both consistent with underestimation of N. As with the results of the voltage mode measurements before, an increased Ti and decreased N_2 content can be noted in the multiple detection events, indicating ion dissociation processes and corresponding N loss due to undetectable neutrals. However, due to the relatively small amount of multiple detection events, this effect does not have a large impact on the overall measurement, as it is also evident from the software filtering results. Thus, it can be assumed that the uncertainty despite filtering is due to the high laser pulse energy and associated dissociation processes, while fragments are predominantly detected in the form of single detection events.

As mentioned above, the reflectron of the used LEAP 3000X HR causes problems to verify dissociation processes directly. However, Di Russo et al. [40] showed in their work that under certain circumstances an ion correlation histogram can reveal dissociation processes even with a reflectron-based instrument. Dissociation processes, which take place in or after the reflectron, lead to the formation of two daughter ions from the parent molecule, which differ in their kinetic energy. This leads to different times of flight, which in turn becomes visible as a dissociation track in ion correlation histograms. Fig. 6a shows the ion correlation histogram from the multiple detection events of the laser-assisted measurement using 1.5 nJ. All multiple detection events are represented with two or three ions, considering all possible permutations of the ion pairs (i.e., for an event consisting of three ions m_1, m_2 and m_3, the ion pairs $\{m_1|m_2\}$, $\{m_2|m_3\}$ and $\{m_1|m_3\}$ as well as the corresponding points reflected by the first median were considered). A dissociation track is clearly visible, which leads from the intersection with the first median at 36.7 Da, attributed to Ti_2N^{3+}, the parent molecule, towards the intersections {24.0 Da|62.0 Da} and {62.0 Da|

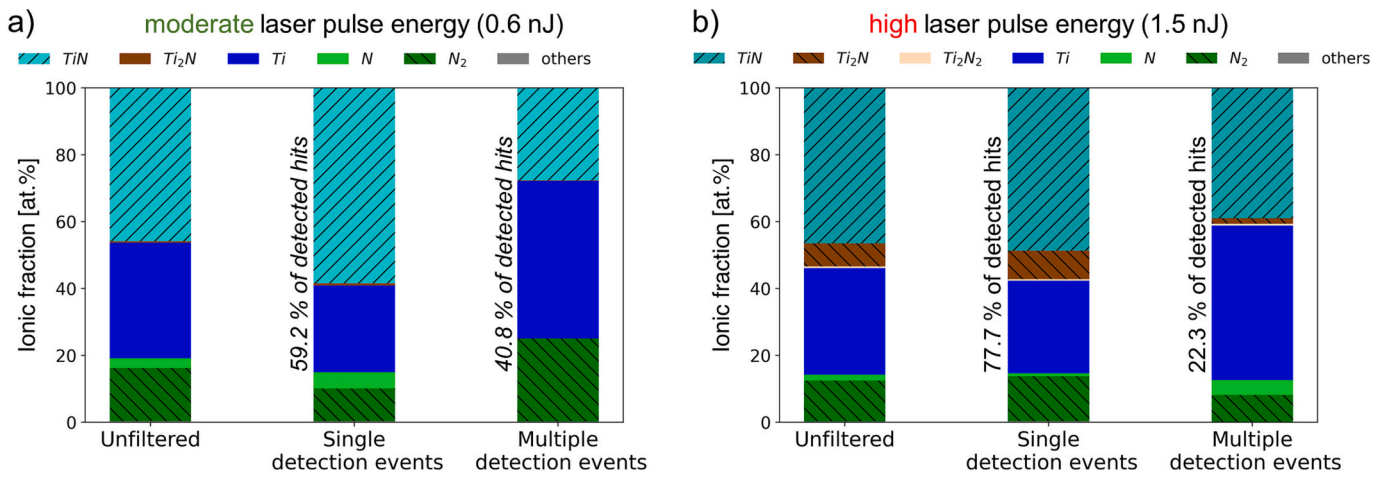

Fig. 5. Analysis of detector events with respect to the ion species that occur using (a) a moderate LPE of 0.6 nJ and (b) a high LPE of 1.5 nJ. In particular, in latter, the large Ti_2N fraction in the single detection events can be seen.

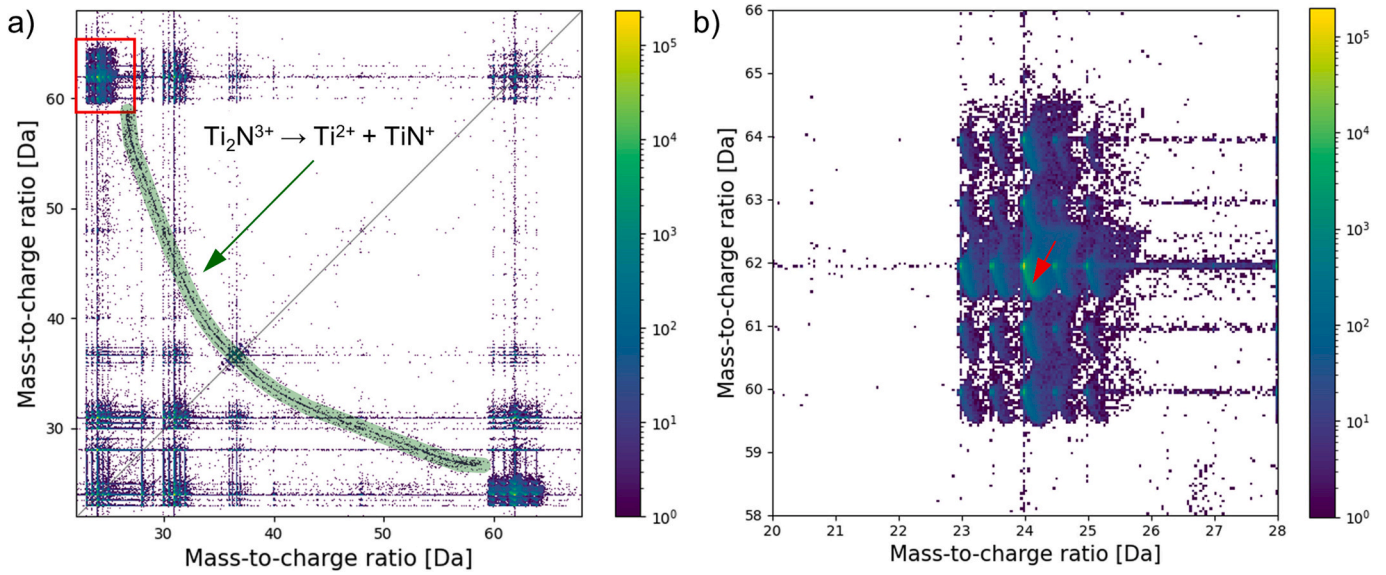

Fig. 6. (a) Ion correlation histogram of TiN from laser-assisted APT measurement using 1.5 nJ. The color bar represents the number of detected ion pairs. The dissociation track is highlighted in green. The red frame marks the section shown in (b). Detail (b) shows the intersection of the two daughter ions Ti^{2+} and TiN^{+}. Some tracks show an intensive negative slope, which is associated to dissociation, those starting from the intersection of the major isotopes are marked with a red arrow. (For interpretation of the references to color in this figure legend, the reader is referred to the web version of this article.)

24.0 Da} corresponding to the daughter ions Ti^{2+} and TiN^{+}. A closer look reveals that the track ends considerably before the intersection point and deviates from the direction; two artifacts that can be traced back to the reflectron [40]. However, the detailed view of the intersection in Fig. 6b reveals intensive compressed tracks whose negative slope is attributable to dissociation. Although it was possible to visualize the dissociation track for $Ti_2N^{3+} \rightarrow Ti^{2+} + TiN^{+}$, it should be noted that there may be other tracks that could not be identified and that it is recommended to study dissociation processes with straight flight path instruments due to the inherent difficulties of interpretation.

3.4. Effect of electric field strength on the measurement accuracy

Exemplary for all evaluations, Fig. 7a and b show the mass spectra of the voltage and laser-assisted (2.0 nJ) measurements with the standard LE, respectively. Highlighted in color are the individual peaks of the different charge states of Ti and the total counts are shown in the corresponding bar chart. While the number of Ti^{3+} and Ti^{2+} ions are similar in the case of the voltage measurement, the number of Ti^{3+} ions decreases considerably in the case of the laser-assisted measurement. Using the post-ionization model of Kingham [41], it is possible to estimate the effective electric field at the apex of the specimen by determining the charge state ratios (CSR), therefore, the total counts were set in relation to each other. In the case of the voltage mode measurement, the Ti^{3+}/Ti^{2+} CSR is 0.93, which corresponds to an average field strength of about 40.0 V/nm during the measurement, which is in good agreement with earlier estimations [42,43]. One problem inevitably encountered in APT measurements of nitrides is the overlap of the peaks of N^{+} and N_2^{2+} at 14 Da. The peak of the ^{15}N isotope, which could be helpful for proper ranging, is below the background due to low natural abundance. At 14.5 Da, no evidence for N_2^{2+} composed of the more abundant ^{14}N and ^{15}N isotopes can be found either. Since the electric field during the measurement was well below 60 V/nm, which is required for the double ionization of N_2 [26], it was assumed that the peak at 14 Da is predominantly composed of N^{+} ions. This assumption was also made for the laser-based APT measurements, since the electric field is even lower due to the additional energy input from the laser.

To get a thorough understanding of the increasing presence of

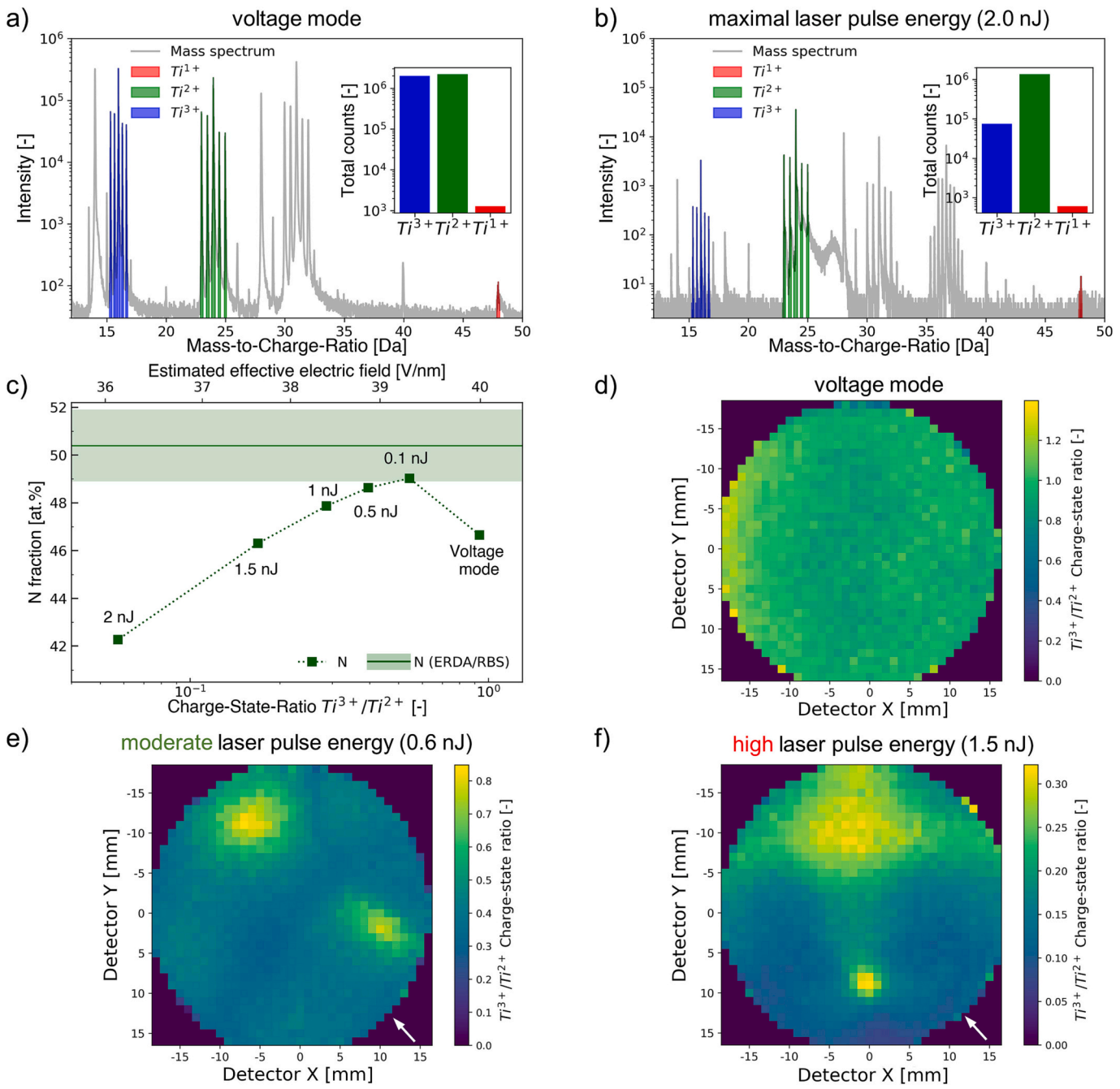

Fig. 7. Mass spectra of (a) the voltage mode and (b) the laser-assisted measurement (2.0 nJ) using a standard LE. Ti peaks, which are used to estimate the effective electric field are marked in different colors. The inserted bar charts represent the total counts of the respective charge states. (c) Evolution of the Ti^{3+}/Ti^{2+} CSR and corresponding electric field with increasing LPE and the observed Ti fraction. The distribution of the Ti^{3+}/Ti^{2+} CSR across the apex surface from the detector's point of view for (d) the voltage mode as well as the laser-assisted measurements applying (e) moderate 0.6 and (f) high 1.5 nJ LPE. In the latter two, the direction of incidence of the laser is indicated by the white arrow at the bottom right. The datasets were sliced in the x-y plane into voxels with a cross-sectional area of 1 × 1 mm^2.

complex molecular ions, such as Ti_2N, with increasing laser pulse energy, the Ti^{3+}/Ti^{2+} CSRs of the measurements were determined and the effective electric fields were estimated. As can be seen in Fig. 7c, the electric field decreases with increasing laser pulse energy and thus, the CSR decreases as well. This behavior related to the thermal energy input by the laser irradiation, enables field evaporation using a lower standing voltage. The results obtained for the N fraction of the corresponding measurements are also shown. From the results, it can be deduced that the compositional accuracy is highly dependent on the electric field. Lowering the field from 40.0 V/nm, in voltage mode, to 39.3 V/nm using 0.1 nJ LPE results in a reduction of the N deviation from the reference value from 3.8 at.% to 1.4 at.%. This finding is probably related to preferred evaporation of the lower field Ti during pulsing in voltage mode and the associated less likely evaporation of the higher field nitrogen. Preferential evaporation is a common reported issue in studies regarding compositional accuracy [5,16,44]. But while with further increase of the LPE the electric field becomes even smaller, the discrepancy to the reference N content is rising again, finally to 8.1 at.% using 2.0 nJ LPE, corresponding to an electric field of 36.1 V/nm. Due to the incidence of the laser, uneven temperature distributions may occur

at the tip. The fact that this also leads to an uneven distribution of the electric field at the tip has been studied in detail for other materials [12,45]. This observation could also be made in the context of this work. Fig. 7d-f shows the spatial distribution of the Ti^{3+}/Ti^{2+} CSR across the apex for the measurements in voltage mode as well as in laser-assisted mode using moderate (0.6 nJ) as well as high (1.5 nJ) LPE from the detector point of view. The CSR in voltage mode ranges between 0.8 and 1.2, corresponding to an electric field strength of 39.6 and 40.4 V/nm, respectively. No significant gradients are visible, the fluctuations might result from sample geometry or crystallography. Using the laser-assisted mode with 0.6 nJ, lower Ti^{3+}/Ti^{2+} CSRs can be observed, mainly ranging between 0.25 and 0.85 (corresponding to 38.4 and 39.9 V/nm). Crystallography is clearly visible, and the field strength is varying in a broader range. The thermal influence of the laser becomes particularly clear when a high LPE of 1.5 nJ is applied, an asymmetric distribution with a severely lowered local electric field of 35.9 V/nm in the area of laser incidence (referred to a Ti^{3+}/Ti^{2+} CSR of 0.05) as well as a significantly higher local electric field (38.5 V/nm) on the shadow side. Based on the significant differences, it cannot be ruled out that this may lead to negative artifacts that could bias the compositional accuracy. In good agreement with the results of Di Russo et al. for GaN [16] and Hans et al. for (Ti,Al)N [6], it can be assumed that with increasing LPE the electric field is insufficient to ionize neutral fragments, resulting from dissociation processes at the surface. Molecular ions that dissociate during flight, on the other hand, have sufficient kinetic energy to leave the environment of the apex of the specimen, but do not reach the detector due to the unguided movement or have insufficient energy to be detected properly [26]. Increasing amounts of non-re-ionized fragments cause the products from dissociation processes to be increasingly detected as single detection events rather than multiple detection events. Thus, it is recommended to apply the lowest possible LPE in order to achieve a maximum electric field during the measurement, while still profiting from the benefits of laser-assisted APT [4].

3.5. Spatial evolution considerations

So far, the characteristic of the hit behavior as well as the evolution of the electric field during the measurements have been considered globally. In order to explore possible lateral effects caused by e.g. raised standing voltage or increased tip radius, the .epos files of the reconstructions were binned along the z-axis with a width of 1 nm and analyzed with respect to the corresponding number of different detection events. Fig. 8a and b show the absolute number and the relative proportion of single and multiple detection events along the z-axis during the voltage mode and laser-assisted APT measurement with the standard LE, respectively. The areas marked using red dashed trapezoids correspond to the examined volumes, since the analysis included only full cross-section volumes, i.e. the volume with constantly increasing diameter excluding the calotte at the end of the reconstruction. As expected from the globally viewed results, in the voltage mode measurement the multiple detection events dominated, whereas in the laser-assisted measurement the majority of detection events consisted of single detection events. The relative proportions are approximately constant throughout the measurements. The average values for the proportion of multiple detection events, 78.8 % and 40.6 % for the voltage mode and laser-assisted APT measurements, respectively, are in very good agreement with the values determined previously by filtering (see Tables 1 and 2). The analysis shows that regardless of the type of measurement, the characteristics of the hit behavior are not significantly altered during a measurement. Therefore, any filtering of multiple detection events, whether software or hardware based, is not assumed to introduce negative spatial artifacts of the evaluated elemental composition. The Ti^{3+}/Ti^{2+} CSRs were used for the estimation of the electric fields, a high number of total evaluated hits enhances the accuracy, thus, the entire measurements were analyzed to obtain good statistics. However, the basic prerequisite for this approach is a stable evaporation

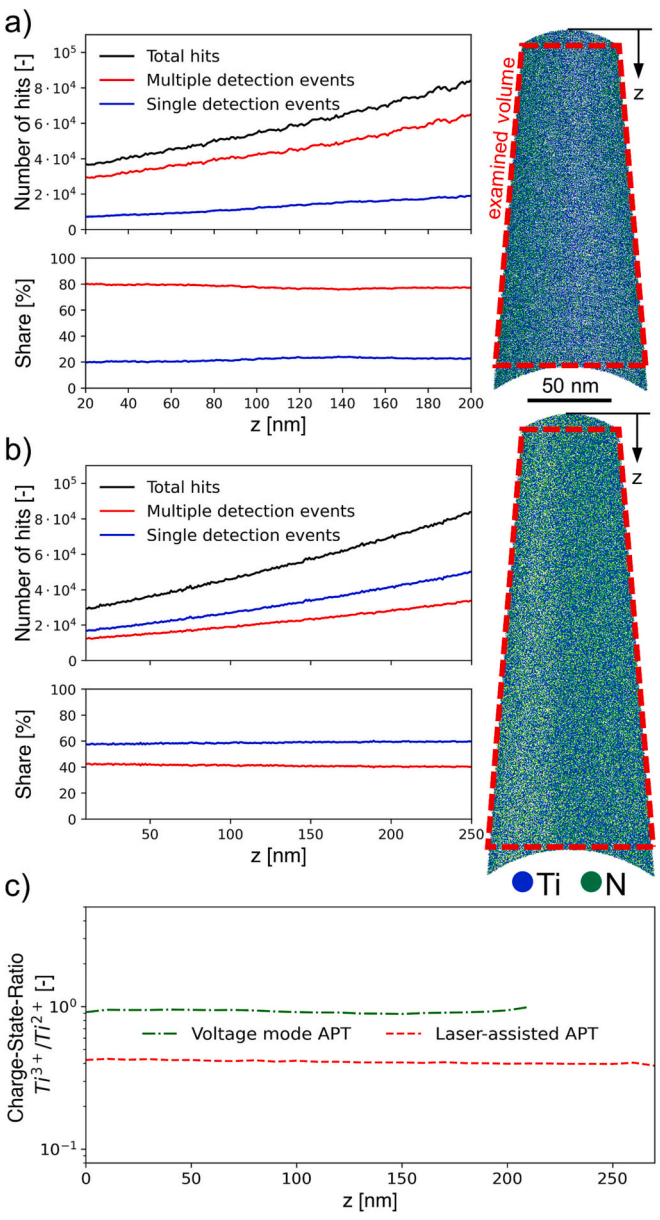

Fig. 8. Analysis of detection events along z-axis during (a) the voltage mode and (b) the laser-assisted APT measurement (0.6 nJ) utilizing a standard LE. The analyzed volume is marked by the red dashed trapezoid. (c) Evolution of charge-state ratios Ti^{3+}/Ti^{2+} along the z-axis during voltage mode as well as laser-assisted measurement (0.6 nJ) with standard LE. The constant ratios indicate that the effective electric fields were also constant during the measurements. (For interpretation of the references to color in this figure legend, the reader is referred to the web version of this article.)

behavior maintaining, a constant electric field. For this purpose, the .pos files of the reconstructions were cut into equidistant slices of 10 nm thickness and the CSR within these was determined by analyzing the mass spectrum. Fig. 8c shows the evolution of the two CSRs along the z-axis, comparing the voltage mode and the slightly larger laser-assisted APT (0.6 nJ) dataset. Since the CSR does not exhibit large variations in either the voltage mode or the laser-assisted APT measurement, it can be deduced that the electric field was constant during the measurements. Thus, the prerequisite for a global consideration is fulfilled.

4. Conclusions

In this study, the influence of multiple detection events on the

accuracy of the elemental composition of a TiN coating using voltage and laser-assisted APT was systematically investigated. The results of complementary ToF-ERDA and RBS were used as reference compositions, which unveiled a stoichiometric composition. It has been shown that filtering multiple detection events, when using voltage mode APT has a strong positive effect on elemental accuracy. By analyzing the datasets filtered by software, the occurred ion species could be compared and the voltage mode measurements indicated dissociation processes, whereby a large fraction of N is apparently lost in the form of neutrals. Using laser-assisted APT, the accuracy was significantly increased, through software filtering the same value could be observed with 0.6 nJ LPE within the measurement uncertainties of ToF-ERDA/RBS. However, the investigations of the laser-assisted APT measurements indicated that a high proportion of multiple detection events per se is not responsible for high deviations from the reference composition. By estimating the electric fields, it was shown that this was 40.0 V/nm for the voltage mode measurement and solely 36.1 V/nm using 2.0 nJ in the laser-assisted mode, suggesting that the field strength is not sufficient to re-ionize fragments from dissociation processes, for instance, which would result in the observed lower fraction of multiple detection events. In the spatial evolution considerations, it could be shown that in the course of the measurements neither the proportions of the detection events nor the electric field changed, thus enabling a global consideration. The presented work contributes significantly to a better understanding and more accurate results in APT measurements of transition metal nitrides.

CRediT authorship contribution statement

Maximilian Schiester: Writing – original draft, Visualization, Software, Methodology, Investigation, Formal analysis, Conceptualization. **Helene Waldl:** Writing – review & editing, Investigation, Formal analysis. **Marcus Hans:** Writing – review & editing, Investigation, Funding acquisition, Formal analysis, Conceptualization. **Mattias Thuvander:** Writing – review & editing, Investigation, Formal analysis. **Daniel Primetzhofer:** Writing – review & editing, Investigation, Formal analysis. **Nina Schalk:** Writing – review & editing, Supervision, Funding acquisition. **Michael Tkadletz:** Writing – review & editing, Supervision, Investigation, Funding acquisition, Formal analysis, Conceptualization.

Declaration of competing interest

The authors declare that they have no known competing financial interests or personal relationships that could have appeared to influence the work reported in this paper.

Data availability

Data will be made available on request.

Acknowledgements

The authors want to thank Christian Saringer for his contribution to programming the scripts. The authors gratefully acknowledge the financial support under the scope of the COMET program within the K2 Center “Integrated Computational Material, Process and Product Engineering (IC-MPPE)” (Project No 886385). This program is supported by the Austrian Federal Ministries for Climate Action, Environment, Energy, Mobility, Innovation and Technology (BMK) and for Labour and Economy (BMAW), represented by the Austrian Research Promotion Agency (FFG), and the federal states of Styria, Upper Austria and Tyrol. The financial support by the Austrian Federal Ministry for Digital and Economic Affairs and the National Foundation for Research, Technology and Development is gratefully acknowledged. The financial support by the Austrian Federal Ministry of Labour and Economy, the National Foundation for Research, Technology and Development and the Christian Doppler Research Association is gratefully acknowledged. Transnational access to the ion beam analysis facility at Uppsala University has been supported by the RADIATE project under the Grant Agreement 824096 from the EU Research and Innovation program HORIZON 2020. Accelerator operation at Uppsala University has been supported by the Swedish research council VR-RFI (#2019-00191).

Appendix A. Supplementary data

Supplementary data to this article can be found online at https://doi.org/10.1016/j.surfcoat.2023.130318.

References

[1] E.W. Müller, Field desorption, Phys. Rev. 102 (1956) 618–624, https://doi.org/10.1103/PhysRev.102. 618.
[2] E.W. Müller, J.A. Panitz, S.B. McLane, The atom-probe field ion microscope, Rev. Sci. Instrum. 39 (1968) 83–86, https://doi.org/10.1063/1.1683116.
[3] D. Blavette, A. Bostel, J.M. Sarrau, B. Deconihout, A. Menand, An atom probe for three-dimensional tomography, Nature 363 (1993) 432–435, https://doi.org/10.1038/363432a0.
[4] B. Gault, F. Vurpillot, A. Vella, M. Gilbert, A. Menand, D. Blavette, B. Deconihout, Design of a femtosecond laser assisted tomographic atom probe, Rev. Sci. Instrum. 77 (2006), https://doi.org/10.1063/1.2194089.
[5] M. Hans, J.M. Schneider, On the chemical composition of TiAlN thin films - comparison of ion beam analysis and laser-assisted atom probe tomography with varying laser pulse energy, Thin Solid Films 688 (2019), 137251, https://doi.org/10.1016/j.tsf.2019.04.026.
[6] M. Hans, J.M. Schneider, Electric field strength-dependent accuracy of TiAlN thin film composition measurements by laser-assisted atom probe tomography, New J. Phys. 22 (2020), https://doi.org/10.1088/1367-2630/ab7770.
[7] A. Devaraj, D.E. Perea, J. Liu, L.M. Gordon, T.J. Prosa, P. Parikh, D.R. Diercks, S. Meher, R.P. Kolli, Y.S. Meng, S. Thevuthasan, Three-dimensional nanoscale characterisation of materials by atom probe tomography, Int. Mater. Rev. 63 (2018) 68–101, https://doi.org/10.1080/0 9506608.2016.1270728.
[8] F. Tang, B. Gault, S.P. Ringer, J.M. Cairney, Optimization of pulsed laser atom probe (PLAP) for the analysis of nanocomposite Ti-Si-N films, Ultramicroscopy 110 (2010) 836–843, https://doi.org/10.1016/j.ultramic.2010.03.003.
[9] M. Tkadletz, N. Schalk, R. Daniel, J. Keckes, C. Czettl, C. Mitterer, Advanced characterization methods for wear resistant hard coatings: a review on recent progress, Surf. Coat. Technol. 285 (2016) 31–46, https://doi.org/10.1016/j.surfcoat.2015.11.016.
[10] H.S. Kitaguchi, S. Lozano-Perez, M.P. Moody, Quantitative analysis of carbon in cementite using pulsed laser atom probe, Ultramicroscopy 147 (2014) 51–60, https://doi.org/10.1016/j.ultramic.2014.06.004.
[11] T.L. Martin, A.J. London, B. Jenkins, S.E. Hopkin, J.O. Douglas, P.D. Styman, P.A. J. Bagot, M.P. Moody, Comparing the consistency of atom probe tomography measurements of small-scale segregation and clustering between the LEAP 3000 and LEAP 5000 instruments, Microsc. Microanal. 23 (2017) 227–237, https://doi.org/10.1017/S1431927617000356.
[12] R. Cuduvally, R.J.H. Morris, P. Ferrari, J. Bogdanowicz, C. Fleischmann, D. Melkonyan, W. Vandervorst, Potential sources of compositional inaccuracy in the atom probe tomography of InxGa1-xAs, Ultramicroscopy 210 (2020), 112918, https://doi.org/10.1016/j.ultramic.2019. 112918.
[13] D. Santhanagopalan, D.K. Schreiber, D.E. Perea, R.L. Martens, Y. Janssen, P. Khalifah, Y.S. Meng, Effects of laser energy and wavelength on the analysis of LiFePO4 using laser assisted atom probe tomography, Ultramicroscopy 148 (2015) 57–66, https://doi.org/10.1016/j.ultramic.2014. 09.004.
[14] E. Di Russo, I. Blum, J. Houard, G. Da Costa, D. Blavette, L. Rigutti, Field-dependent measurement of GaAs composition by atom probe tomography, Microsc. Microanal. 23 (2017) 1067–1075, https://doi.org/10.1017/S1431927617012582.
[15] H. Waldl, M. Hans, M. Schiester, D. Primetzhofer, M. Burtscher, N. Schalk, M. Tkadletz, Decomposition of CrN induced by laser-assisted atom probe tomography, Ultramicroscopy 246 (2023), 113673, https://doi.org/10.1016/j.ultramic.2022.113673.
[16] E. Di Russo, I. Blum, J. Houard, M. Gilbert, G. Da Costa, D. Blavette, L. Rigutti, Compositional accuracy of atom probe tomography measurements in GaN: impact of experimental parameters and multiple evaporation events, Ultramicroscopy 187 (2018) 126–134, https://doi.org/10.1016/j.ultramic.2018.02.001.
[17] L. Rigutti, L. Mancini, D. Hernández-Maldonado, W. Lefebvre, E. Giraud, R. Butté, J.F. Carlin, N. Grandjean, D. Blavette, F. Vurpillot, Statistical correction of atom probe tomography data of semiconductor alloys combined with optical spectroscopy: the case of Al0.25Ga0.75N, J. Appl. Phys. 119 (2016), 105704, https://doi.org/10.1063/1.4943612.
[18] J. Angseryd, F. Liu, H.O. Andren, S.S.A. Gerstl, M. Thuvander, Quantitative APT analysis of Ti(C,N), Ultramicroscopy 111 (2011) 609–614, https://doi.org/10.1016/j.ultramic.2011.01.031.
[19] M. Thuvander, G. Östberg, M. Ahlgren, L.K.L. Falk, Atom probe tomography of a Ti-Si-Al-C-N coating grown on a cemented carbide substrate, Ultramicroscopy 159 (2015) 308–313, https://doi.org/10.1016/j.ultramic.2015.04.008.

[20] R.J.H. Morris, R. Cuduvally, J.R. Lin, M. Zhao, W. Vandervorst, M. Thuvander, C. Fleischmann, Field dependent study on the impact of co-evaporated multihits and ion pile-up for the apparent stoichiometric quantification of GaN and AlN, Ultramicroscopy 241 (2022), 113592, https://doi.org/10.1016/j.ultramic.2022.113592.
[21] L. Mancini, N. Amirifar, D. Shinde, I. Blum, M. Gilbert, A. Vella, F. Vurpillot, W. Lefebvre, R. Lardé, E. Talbot, P. Pareige, X. Portier, A. Ziani, C. Davesnne, C. Durand, J. Eymery, R. Butté, J.F. Carlin, N. Grandjean, L. Rigutti, Composition of wide bandgap semiconductor materials and nanostructures measured by atom probe tomography and its dependence on the surface electric field, J. Phys. Chem. C 118 (2014) 24136–24151, https://doi.org/10.1021/jp5071264.
[22] R.J.H. Morris, R. Cuduvally, D. Melkonyan, C. Fleischmann, M. Zhao, L. Arnoldi, P. van der Heide, W. Vandervorst, Toward accurate composition analysis of GaN and AlGaN using atom probe tomography, J. Vac. Sci. Technol., B: Nanotechnol. Microelectron.: Mater., Process., Meas., Phenom. 36 (2018), https://doi.org/10.1116/1.5019693.
[23] Z. Peng, F. Vurpillot, P.P. Choi, Y. Li, D. Raabe, B. Gault, On the detection of multiple events in atom probe tomography, Ultramicroscopy 189 (2018) 54–60, https://doi.org/10.1016/j. ultramic.2018.03.018.
[24] G. Da Costa, H. Wang, S. Duguay, A. Bostel, D. Blavette, B. Deconihout, Advance in multi-hit detection and quantization in atom probe tomography, Rev. Sci. Instrum. 83 (2012), https://doi.org/10.1063/1.4770120.
[25] F. Meisenkothen, E.B. Steel, T.J. Prosa, K.T. Henry, R. Prakash Kolli, Effects of detector dead-time on quantitative analyses involving boron and multi-hit detection events in atom probe tomography, Ultramicroscopy 159 (2015) 101–111, https://doi.org/10.1016/j.ultramic.2015.07. 009.
[26] B. Gault, D.W. Saxey, M.W. Ashton, S.B. Sinnott, A.N. Chiaramonti, M.P. Moody, D. K. Schreiber, Behavior of molecules and molecular ions near a field emitter, New J. Phys. 18 (2016), https://doi.org/10.1088/1367-2630/18/3/033031.
[27] M. Thuvander, A. Kvist, L.J.S. Johnson, J. Weidow, H.O. Andrén, Reduction of multiple hits in atom probe tomography, Ultramicroscopy 132 (2013) 81–85, https://doi.org/10.1016/j.ultramic. 2012.12.005.
[28] M. Thuvander, D. Shinde, A. Rehan, S. Ejnermark, K. Stiller, Improving compositional accuracy in APT analysis of carbides using a decreased detection efficiency, Microsc. Microanal. 25 (2019) 454–461, https://doi.org/10.1017/S1431927619000424.
[29] M. Tkadletz, A. Lechner, S. Pölzl, N. Schalk, Anisotropic wet-chemical etching for preparation of freestanding films on Si substrates for atom probe tomography: a simple yet effective approach, Ultramicroscopy 230 (2021) 0–3, https://doi.org/10.1016/j.ultramic.2021.113402.
[30] P. Ström, D. Primetzhofer, Ion beam tools for nondestructive in-situ and in-operando composition analysis and modification of materials at the Tandem Laboratory in Uppsala, J. Instrum. 17 (2022), https://doi.org/10.1088/1748-0221/17/04/P04011.
[31] M.V. Moro, R. Holeňák, L. Zendejas Medina, U. Jansson, D. Primetzhofer, Accurate high-resolution depth profiling of magnetron sputtered transition metal alloy films containing light species: a multi-method approach, Thin Solid Films 686 (2019), https://doi.org/10.1016/j.tsf.2019.137416.
[32] M. Hans, M. Tkadletz, D. Primetzhofer, H. Waldl, M. Schiester, M. Bartosik, C. Czettl, N. Schalk, C. Mitterer, J.M. Schneider, Is it meaningful to quantify vacancy concentrations of nanolamellar (Ti,Al)N thin films based on laser-assisted atom probe data? Surf. Coat. Technol. 130020 (2023) https://doi.org/10.1016/j.surfcoat.2023.130020.
[33] K. Thompson, D. Lawrence, D.J. Larson, J.D. Olson, T.F. Kelly, B. Gorman, In situ site-specific specimen preparation for atom probe tomography, Ultramicroscopy 107 (2007) 131–139, https://doi.org/10.1016/j.ultramic.2006.06.008.
[34] M.K. Miller, K.F. Russell, Atom probe specimen preparation with a dual beam SEM/FIB miller, Ultramicroscopy 107 (2007) 761–766, https://doi.org/10.1016/j.ultramic.2007.02.023.
[35] D.J. Larson, T.J. Prosa, R.M. Ulfig, B.P. Geiser, T.F. Kelly, Local Electrode Atom Probe Tomography, 3rd ed., 2013.
[36] F. De Geuser, B. Gault, Metrology of small particles and solute clusters by atom probe tomography, Acta Mater. 188 (2020) 406–415, https://doi.org/10.1016/j.actamat.2020.02.023.
[37] D.W. Saxey, Correlated ion analysis and the interpretation of atom probe mass spectra, Ultramicroscopy 111 (2011) 473–479, https://doi.org/10.1016/J.ULTRAMIC.2010.11.021.
[38] A. Cerezo, T.J. Godfrey, S.J. Sijbrandij, G.D.W. Smith, P.J. Warren, Performance of an energy-compensated three-dimensional atom probe, Rev. Sci. Instrum. 69 (1998) 49–58, https://doi.org/10.1063/1.1148477.
[39] F. De Geuser, B. Gault, A. Bostel, F. Vurpillot, Correlated field evaporation as seen by atom probe tomography, Surf. Sci. 601 (2007) 536–543, https://doi.org/10.1016/j.susc.2006.10.019.
[40] E. Di Russo, I. Blum, I. Rivalta, J. Houard, G. Da Costa, F. Vurpillot, D. Blavette, L. Rigutti, Detecting dissociation dynamics of phosphorus molecular ions by atom probe tomography, J. Phys. Chem. A 124 (2020) 10977–10988, https://doi.org/10.1021/acs.jpca.0c09259.
[41] D.R. Kingham, The post-ionization of field evaporated ions: a theoretical explanation of multiple charge states, Surf. Sci. 116 (1982) 273–301, https://doi.org/10.1016/0039-6028(82)90434-4.
[42] L.J.S. Johnson, M. Thuvander, K. Stiller, M. Odén, L. Hultman, Spinodal decomposition of Ti 0.33Al 0.67N thin films studied by atom probe tomography, Thin Solid Films 520 (2012) 4362–4368, https://doi.org/10.1016/j.tsf.2012.02.085.
[43] M. Tkadletz, C. Hofer, C. Wüstefeld, N. Schalk, M. Motylenko, D. Rafaja, H. Holzschuh, W. Bürgin, B. Sartory, C. Mitterer, C. Czettl, Thermal stability of nanolamellar fcc-Ti1-xAlxN grown by chemical vapor deposition, Acta Mater. 174 (2019) 195–205, https://doi.org/10.1016/j. actamat.2019.05.044.
[44] G. Sha, S.P. Ringer, Effect of laser pulsing on the composition measurement of an Al-Mg-Si-Cu alloy using three-dimensional atom probe, Ultramicroscopy 109 (2009) 580–584, https://doi.org/10.1016/j.ultramic.2008.10.012.
[45] G. Sha, A. Cerezo, G.D.W. Smith, Field evaporation behavior during irradiation with picosecond laser pulses, Appl. Phys. Lett. 92 (2008) 2006–2009, https://doi.org/10.1063/1.2837626.